

# QCD diffractive mechanism of exclusive $W^+W^-$ pair production at high energies

Piotr Lebiedowicz,<sup>1,\*</sup> Roman Pasechnik,<sup>2,†</sup> and Antoni Szczurek<sup>3,1,‡</sup>

<sup>1</sup>*Institute of Nuclear Physics PAN, PL-31-342 Cracow, Poland*

<sup>2</sup>*Department of Astronomy and Theoretical Physics,  
Lund University, SE-223 62 Lund, Sweden*

<sup>3</sup>*University of Rzeszów, PL-35-959 Rzeszów, Poland*

## Abstract

We discuss new diffractive mechanism of central exclusive production of  $W^+W^-$  pairs in proton-proton collisions at the LHC. We include diagrams with intermediate virtual Higgs boson as well as quark box diagrams. Several observables related to this process are calculated. Predictions for the total cross section and differential distributions in  $W$ -boson rapidity and transverse momentum as well as  $WW$  invariant mass are presented. We also show results for different polarization states of the final  $W^\pm$  bosons. We compare the contribution of the  $\gamma\gamma \rightarrow W^+W^-$  mechanism considered in the literature with the contribution of the diffractive mechanism through the  $gg \rightarrow W^+W^-$  subprocess for the different observables. The phase space integrated diffractive contribution when separated is only a small fraction of fb compared to 115.4 fb of the  $\gamma\gamma$ -contribution without absorption. The latter contribution dominates at small four-momentum transfers squared in the proton lines and in a broad range of  $W^+W^-$  invariant masses. This offers a possibility of efficient searches for anomalous triple-boson ( $\gamma WW$ ) and quartic-boson ( $\gamma\gamma WW$ ) couplings and testing models beyond the Standard Model. We discuss shortly also the  $pp \rightarrow pp\gamma\gamma$  process, where the box contribution is very similar to that for  $W^+W^-$  and compare our results with recent CDF data. Nice agreement has been achieved without additional free parameters.

PACS numbers: 13.85.-t, 13.87.Ce, 14.70.Fm

---

\*Electronic address: Piotr.Lebiedowicz@ifj.edu.pl

†Electronic address: Roman.Pasechnik@thep.lu.se

‡Electronic address: Antoni.Szczurek@ifj.edu.pl

## I. INTRODUCTION

The central exclusive production (CEP) process  $pp \rightarrow p + X + p$ , where  $X$  stands for a centrally produced system separated from the two very forward protons by large rapidity gaps, has been proposed in Refs. [1, 2] as an alternative way of searching for the neutral Higgs boson (see Ref. [3] for a review). If momenta of the outgoing protons are measured by forward proton detectors placed at 220 m and 420 m from the ATLAS/CMS interaction point [4], the mass of the  $X$  system may be reconstructed [5] with very precise resolution.

The exclusive reaction  $pp \rightarrow pHp$  has been intensively studied by the Durham group [6] in the last decade. This study was motivated by the clean environment and largely reduced background due to a suppression of  $b\bar{b}$  production as a consequence of the spin-parity conservation in the forward limit. However, very recent precise calculations of Refs. [7] have shown that the situation with Higgs CEP background in the  $b\bar{b}$  channel is more complicated and the signal is to a large extent shadowed by the exclusive non-reducible continuum  $b\bar{b}$  production. In addition, reducible backgrounds from a misidentification of gluonic jets as  $b$ -quark jets can be very difficult to separate [8]. Since the total cross section for the Higgs CEP is quite small and rather uncertain, the issue with the Higgs CEP is still far from its final resolution, from both theoretical and experimental point of view.

The final system  $X$  in the midrapidity region is predominantly produced in the  $J_z = 0$  state as dictated by the well-known  $J_z = 0$  selection rule [6]. However, corrections to this rule due to slightly off-forward protons can be important for lower (a few GeV) mass central systems and may lead to sizeable contributions in the observable signals, in particular, in the  $\chi_c$  mesons [9, 10],  $b\bar{b}$  [7] and  $gg$  [8, 11] CEP. The emission of gluons from the "screening" gluon could also violate the  $J_z = 0$  selection rule as has recently been emphasized in Ref. [11].

In order to reduce the theoretical uncertainties of the CEP mechanism, coming from both the hard subprocess (Sudakov form factor [11, 12], next-to-leading order QCD corrections [13]) and the soft interactions (color screening effects at extremely small gluon  $x$  [14], rapidity gap survival factor [15], poorly known unintegrated gluon distribution functions (UGDFs) at small gluon  $q_\perp$  and  $x$  [9, 10]), new experimental data on various exclusive production channels are certainly required and expected to come soon from ongoing LHC measurements. In particular, as it was stressed e.g. in Ref. [12] the measurements of the exclusive dijets production at the LHC could largely reduce the theoretical uncertainty in the Higgs boson CEP. Other measurements, e.g. heavy quarkonia [9, 10],  $\gamma\gamma$  [10], high- $p_\perp$  light mesons [16, 17], associated charged Higgs  $H^+W^-$  [18] CEP, etc., are also important in this context. Some of these results have been compared to experimental data from the Tevatron [19, 20], and a rough quantitative agreement between them has been achieved.

In this paper, we focus on exclusive production of  $W^+W^-$  pairs in high-energy proton-proton collisions. It was found recently [21, 22] that the reaction is an ideal case to study experimentally  $\gamma W^+W^-$  and  $\gamma\gamma W^+W^-$  couplings<sup>1</sup>.

The  $\gamma\gamma \rightarrow W^+W^-$  process is interesting reaction to test the Standard Model and any other theory beyond the Standard Model. The linear collider would be a good option to study the couplings of gauge bosons in the distant future. For instance in Ref.[24] the anomalous coupling in locally  $SU(2) \times U(1)$  invariant effective Lagrangian was studied. Other models also lead to anomalous gauge boson coupling.

The photon-photon contribution for the purely exclusive production of  $W^+W^-$  was con-

---

<sup>1</sup> Some more subtle aspects of the beyond Standard Model anomalous couplings were discussed e.g. in [23].

sidered so far in the literature. The diffractive production and decay of Higgs boson into the  $W^+W^-$  pair was discussed in Ref. [25], and the corresponding cross section turned out to be significantly smaller than that for the  $\gamma\gamma$ -contribution. Provided this is the case, the  $W^+W^-$  pair production signal would be particularly sensitive to New Physics contributions in the  $\gamma\gamma \rightarrow W^+W^-$  subprocess [21, 22]. Similar analysis has been considered recently for  $\gamma\gamma \rightarrow ZZ$  [26]. These previous analyses strongly motivate our present detailed study on a competitive diffractive contribution. The  $pp \rightarrow pW^+W^-p$  process going through the diffractive QCD mechanism with the  $gg \rightarrow W^+W^-$  subprocess naturally constitutes a background for the exclusive electromagnetic  $pp \rightarrow p(\gamma\gamma \rightarrow W^+W^-)p$  process. We consider not only the mechanism with intermediate Higgs boson but also quark box contributions never estimated in exclusive processes. Both the Higgs and box contribution may interfere together. We discuss here the interference effects. Corresponding measurements will be possible to perform at the ATLAS detector with the use of very forward proton detectors [21]. In order to quantify to what extent the QCD mechanism competes with the “signal” from the  $\gamma\gamma$  fusion, we calculate both contributions and compare them differentially as a function of several relevant kinematical variables.

Since the box contribution of exclusive diffractive  $pp \rightarrow ppW^+W^-$  process is very similar to the  $p\bar{p} \rightarrow p\bar{p}\gamma\gamma$  process which has been measured recently [20], we discuss the latter one and compare corresponding results with the recent CDF data.

## II. DIFFRACTIVE MECHANISM OF EXCLUSIVE $W^+W^-$ PAIR PRODUCTION

A schematic diagram for central exclusive production of  $W^\pm W^\mp$  pairs in proton-proton scattering  $pp \rightarrow pW^\pm W^\mp p$  is shown in Fig. 1. Similar mechanisms have been considered in inclusive production of  $W^+W^-$  pairs (see e.g. Refs. [27, 29, 30]). In what follows, we use the standard theoretical description of CEP processes developed by Khoze, Martin and Ryskin for the exclusive production of Higgs boson [6].

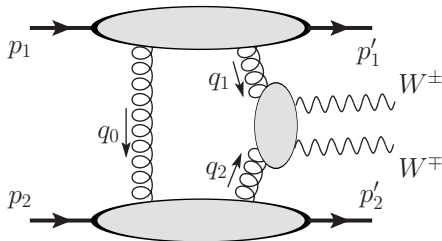


FIG. 1: Generic diagram for the central exclusive  $WW$  pair production in  $pp$  collisions. Momenta of incident particles are shown explicitly.

The momenta of intermediate gluons are given by Sudakov decompositions in terms of the incoming proton four-momenta  $p_{1,2}$

$$\begin{aligned} q_1 &= x_1 p_1 + q_{1\perp}, & q_2 &= x_2 p_2 + q_{2\perp}, & 0 < x_{1,2} < 1, \\ q_0 &= x' p_1 - x' p_2 + q_{0\perp} \simeq q_{0\perp}, & x' &\ll x_{1,2}, \end{aligned} \quad (2.1)$$

where  $x_{1,2}, x'$  are the longitudinal momentum fractions for active (fusing) and color screening gluons, respectively.

In the forward proton scattering limit, we have

$$\begin{aligned} t_{1,2} &= (p_{1,2} - p'_{1,2})^2 \simeq p_{1,2\perp}^2 \rightarrow 0, \\ q_{\perp} &\equiv q_{0\perp} \simeq -q_{1\perp} = q_{2\perp}. \end{aligned} \quad (2.2)$$

The QCD factorisation of the process at the hard scale  $\mu_F$  is provided by the large invariant mass of the  $WW$  pair  $M_{WW}$ , i.e.

$$\mu_F^2 \equiv s x_1 x_2 \simeq M_{WW}^2. \quad (2.3)$$

It is convenient to introduce the Sudakov expansion for  $W^{\pm}$  boson momenta

$$k_+ = x_1^+ p_1 + x_2^+ p_2 + k_{+\perp}, \quad k_- = x_1^- p_1 + x_2^- p_2 + k_{-\perp} \quad (2.4)$$

leading to

$$x_{1,2} = x_{1,2}^+ + x_{1,2}^-, \quad x_{1,2}^+ = \frac{m_{+\perp}}{\sqrt{s}} e^{\pm y_+}, \quad x_{1,2}^- = \frac{m_{-\perp}}{\sqrt{s}} e^{\pm y_-}, \quad m_{\pm\perp}^2 = m_W^2 + |\mathbf{k}_{\pm\perp}|^2, \quad (2.5)$$

in terms of  $W^{\pm}$  rapidities  $y_{\pm}$  and transverse masses  $m_{\pm\perp}$ . For simplicity, in actual calculations we work in the forward limit given by Eq. (2.2), which implies that  $\mathbf{k}_{+\perp} = -\mathbf{k}_{-\perp}$ .

In actual calculations below,  $W^{\pm}$  bosons are assumed to be on-mass-shell, whereas particular contributions to the observables can then be estimated in the narrow-width approximation. For example, in the leptonic channel we have the following observable cross section

$$\sigma_{l^+\nu l^-\nu} \simeq \sigma_{WW} \times \text{BR}(W^+ \rightarrow l^+\nu) \text{BR}(W^- \rightarrow l^-\nu), \quad (2.6)$$

where  $\text{BR}(W^+ \rightarrow l^+\nu) = (10.80 \pm 0.09) \times 10^{-2}$  [31] for a given lepton flavor. Both electrons and muons can be used in practice [21].

We write the amplitude of the diffractive process, which at high energy is dominated by its imaginary part, as

$$\mathcal{M}_{\lambda_+\lambda_-}(s, t_1, t_2) \simeq is \frac{\pi^2}{2} \int d^2 \mathbf{q}_{0\perp} V_{\lambda_+\lambda_-}(q_1, q_2, k_+, k_-) \frac{f_g(q_0, q_1; t_1) f_g(q_0, q_2; t_2)}{\mathbf{q}_{0\perp}^2 \mathbf{q}_{1\perp}^2 \mathbf{q}_{2\perp}^2}, \quad (2.7)$$

where  $\lambda_{\pm} = \pm 1, 0$  are the polarisation states of the produced  $W^{\pm}$  bosons, respectively,  $f_g(r_1, r_2; t)$  is the off-diagonal unintegrated gluon distribution function (UGDF), which depends on the longitudinal and transverse components of both gluons momenta. The gauge-invariant  $gg \rightarrow W_{\lambda_+}^+ W_{\lambda_-}^-$  hard subprocess amplitude  $V_{\lambda_+\lambda_-}(q_1, q_2, k_+, k_-)$  is given by the light cone projection

$$V_{\lambda_+\lambda_-} = n_{\mu}^+ n_{\nu}^- V_{\lambda_+\lambda_-, \mu\nu} = \frac{4}{s} \frac{q_{1\perp}^{\mu}}{x_1} \frac{q_{2\perp}^{\nu}}{x_2} V_{\lambda_+\lambda_-, \mu\nu}, \quad q_1^{\mu} V_{\lambda_+\lambda_-, \mu\nu} = q_2^{\nu} V_{\lambda_+\lambda_-, \mu\nu} = 0, \quad (2.8)$$

where  $n_{\mu}^{\pm} = p_{1,2}^{\mu}/E_{p,cms}$  and the center-of-mass proton energy  $E_{p,cms} = \sqrt{s}/2$ . We adopt the definition of gluon transverse polarisation vectors proportional to the transverse gluon momenta  $q_{1,2\perp}$ , i.e.  $\epsilon_{1,2} \sim q_{1,2\perp}/x_{1,2}$ . The helicity matrix element in the previous expression reads

$$V_{\lambda_+\lambda_-}^{\mu\nu}(q_1, q_2, k_+, k_-) = \epsilon^{*\rho}(k_+, \lambda_+) \epsilon^{*\sigma}(k_-, \lambda_-) V_{\rho\sigma}^{\mu\nu}, \quad (2.9)$$

in terms of the Lorentz and gauge invariant  $2 \rightarrow 2$  amplitude  $V_{\rho\sigma}^{\mu\nu}$  and  $W$  boson polarisation vectors  $\epsilon(k, \lambda)$ . Below we will analyze the exclusive production with polarized  $W^+$  or  $W^-$ . In Eq. (2.9)  $\epsilon_\mu(k_+, \lambda_+)$  and  $\epsilon_\nu(k_-, \lambda_-)$  can be defined easily in the proton-proton center-of-mass frame as

$$\begin{aligned}\epsilon(k, 0) &= \frac{E_W}{m_W} \left( \frac{k}{E_W}, \cos \phi \sin \theta, \sin \phi \sin \theta, \cos \theta \right), \\ \epsilon(k, \pm 1) &= \frac{1}{\sqrt{2}} (0, i \sin \phi \mp \cos \theta \cos \phi, -i \cos \phi \mp \cos \theta \sin \phi, \pm \sin \theta),\end{aligned}\quad (2.10)$$

where  $\phi$  is the azimuthal angle of a produced boson, and satisfy  $\epsilon^\mu(\lambda)\epsilon_\mu^*(\lambda) = -1$  and  $\epsilon_\mu^*(k_+, \lambda_+)k_+^\mu = \epsilon_\nu^*(k_-, \lambda_-)k_-^\nu = 0$ . In the forward limit, provided by Eq. (2.2), the azimuthal angles of the  $W^+$  and  $W^-$  bosons are related as  $\phi_- = \phi_+ + \pi$ .

The diffractive amplitude given by Eq. (2.7) is averaged over the color indices and over the two transverse polarizations of the incoming gluons. The relevant color factor which includes summing over colors of quarks in the loop (triangle or box) and averaging over fusing gluon colors (according to the definition of unintegrated gluon distribution function) is the same as in the previously studied Higgs CEP (for more details on derivation of the generic  $pp \rightarrow pXp$  amplitude, see e.g. Ref. [3]). The matrix element  $V_{\lambda_+, \lambda_-}$  contains twice the strong coupling constant  $g_s^2 = 4\pi\alpha_s$ . In our calculation here we take the running coupling constant  $\alpha_s(\mu_{hard}^2 = M_{WW}^2)$  which depends on the invariant mass of  $WW$  pair as a hard renormalisation scale of the process. The choice of the scale approximately introduces roughly a factor of two model uncertainties when varying the hard scale  $\mu_{hard}$  between  $2M_{WW}$  and  $M_{WW}/2$  values.

The bare amplitude above is subjected to absorption corrections that depend on the collision energy and typical proton transverse momenta. As in the original KMR calculations [6], the bare production cross section is usually multiplied by a rapidity gap survival factor which we take the same as for the Higgs boson and  $b\bar{b}$  production to be  $S_g = 0.03$  at the LHC energy (see e.g. Ref. [8]).

### A. The hard subprocess

The typical contributions to the  $gg \rightarrow W^+W^-$  subprocess are shown in Fig. 2. The total number of topologically different loop diagrams amounts to two triangles, and six boxes. In the central exclusive  $W^+W^-$  production, triangle diagrams with  $\gamma$  and  $Z$  bosons in the intermediate state are suppressed due to the  $J_z = 0$  and parity selection rule for singlet gluon-gluon to (virtual) photon transition strictly valid in the on-shell limit of fusing gluons and Landau-Yang theorem for intermediate  $Z$  boson.

Then the only non-zeroth contribution comes from the Higgs resonant diagram, and in the next subsection we will discuss it in detail. However, this can only lead to a sizeable enhancement of the cross section close to its threshold  $m_{h^0} \simeq M_{WW} \gtrsim 2m_W$  [25]. The Standard Model Higgs bosons with such large masses have been recently excluded by the Tevatron [32] and LHC [33, 34] measurements. For yet allowed values of Higgs mass  $115 \text{ GeV} \lesssim m_{h^0} \lesssim 130 \text{ GeV}$ , corresponding contribution to the  $W^+W^-$  channel is far from the Higgs boson resonance and turned out to be suppressed compared to box contributions at low invariant masses. However, due to interference effects at rather large invariant masses  $M_{WW}$  the resonant (triangles) contribution could become comparable to the non-resonant

(boxes) one. Below, for comparison we have calculated box and triangle (through the  $s$ -channel SM Higgs boson exchange) contributions in different phase space regions <sup>2</sup> which could be interesting for future measurements with forward detectors at ATLAS or CMS.

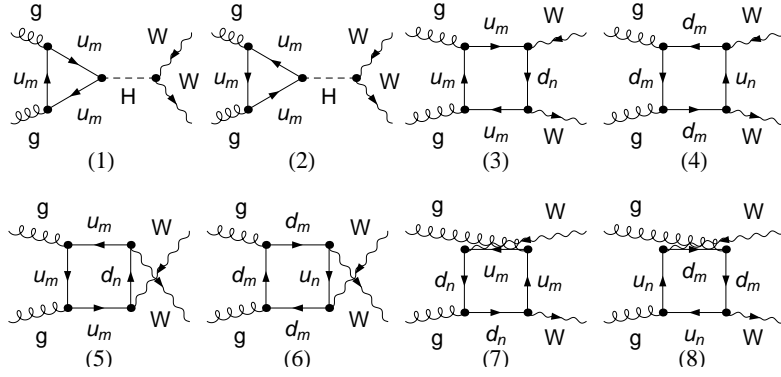


FIG. 2: Representative diagrams of the hard subprocess  $gg \rightarrow W^\pm W^\mp$ , which contribute to the exclusive  $WW$  pair production.

### 1. Higgs contribution

The matrix element for the  $gg \rightarrow h^0 \rightarrow W^+W^-$  transition with intermediate  $s$ -channel Higgs boson exchange (see first two diagrams in Fig. 2) can be written in the narrow-width approximation as

$$V_{gg \rightarrow h^0 \rightarrow W^+W^-}(q_1, q_2, k_+, k_-) = \delta^{(4)}(q_1 + q_2 - k_+ - k_-) \times \\ V_{gg \rightarrow h^0}(q_1, q_2, p_{h^0}) \frac{i}{M_{WW}^2 - m_{h^0}^2 + iM_{WW}\Gamma_{\text{tot}}^h} V_{h^0 \rightarrow W^+W^-}(k_+, k_-, \lambda_+, \lambda_-), \quad (2.11)$$

where the Higgs boson momentum is  $p_{h^0} = q_1 + q_2$ , and the  $\delta$ -function reflects the momentum conservation in the process. In order to get a correct resonant invariant mass distribution, the standard Breit-Wigner Higgs propagator with the total Higgs decay width  $\Gamma_{\text{tot}}^h$ , which can be found e.g. in Ref. [36], is used.

In Eq. (2.11), first the  $gg \rightarrow h^0$  amplitude of the Higgs boson production through the top-quark triangle in the  $k_t$ -factorisation approach can be written as (see e.g. Ref. [37])

$$V_{gg \rightarrow h^0} \simeq \frac{i\delta^{ab}}{v} \frac{\alpha_s(\mu_F^2)}{\pi} (\mathbf{q}_{1\perp} \cdot \mathbf{q}_{2\perp}) \frac{2}{3} \left( 1 + \frac{7}{120} \frac{M_{WW}^2}{m_{\text{top}}^2} \right), \quad v = (G_F \sqrt{2})^{-1/2}. \quad (2.12)$$

The second tree-level  $h^0 \rightarrow W^+W^-$  “decay” amplitude reads:

$$V_{h^0 \rightarrow W^+W^-} \simeq im_W \frac{e}{\sin \theta_W} \epsilon^*(k_+, \lambda_+) \epsilon^*(k_-, \lambda_-), \quad (2.13)$$

<sup>2</sup> Close to the  $WW$ -threshold instability of  $W$  bosons [35] should be included.

where the polarisation vectors in the direction of motion of  $W^+$  and  $W^-$  bosons in the proton-proton center-of-mass frame are used in practical calculations.

Potentially interesting contribution could come from the Higgs resonance if the Higgs mass was close to the  $WW$  production threshold. Similar resonance effects have been considered recently in inclusive [38] and exclusive associated [18] charged Higgs boson production, and large contributions beyond the Standard Model were found. However, the SM Higgs mass  $\sim 160$  GeV has been recently excluded in inclusive searches by the CDF Collaboration at Tevatron [32] and by the ATLAS and CMS Collaborations at LHC [33, 34], so yet realistic SM Higgs boson mass interval  $m_{h^0} \sim 115 - 130$  GeV leads to a suppressed triangles' contribution to exclusive  $W^+W^-$  pair production. In the calculation presented here we take  $m_{h^0} = 120$  GeV. Since the Higgs mass is certainly much smaller than the threshold value a precise value of the Higgs boson mass is not very important. A contribution from an extended Higgs sector beyond the Standard Model [38] could be interesting, but we postpone this issue for a later study.

In this work, we are primarily interested in estimation of dominant box contributions as well as in possible box-triangle interference effects within the Standard Model as potentially important irreducible background for the  $\gamma\gamma \rightarrow W^+W^-$  signal relevant for a precision study of anomalous couplings. Thus, our numerical estimates provide minimal limit for the central exclusive  $WW$  production signal.

## 2. Contribution of box diagrams

The box contributions to the  $gg \rightarrow W^+W^-$  parton level subprocess amplitude (see diagrams No. (3-8) in Fig. 2) for on-shell fusing gluons were calculated analytically by using the Mathematica-based `FormCalc` (FC) [39] package. The complete matrix element was generated automatically by the FC tools in terms of one-loop Passarino-Veltman two-, three- and four-point functions and other internally-defined functions (e.g. gluon and vector bosons polarisation vectors) and kinematical variables.

At the next step, the Fortran code for the matrix element was generated, and then used as an external subroutine in our numerical calculations together with other FC routines setting up the Standard Model parameters, coupling constants and kinematics. Instead of built-in FC polarisation vectors we have used transverse gluon polarisation vectors which enter the projection in Eq. (2.8), and the standard  $W^\pm$  polarisation vectors defined in Eq. (2.10), giving us an access to individual polarisation states of the  $W$  bosons. In accordance with the  $k_t$ -factorisation technique, the gauge invariance of the resulting amplitudes for the on-mass-shell initial gluons is ensured by a projection onto the gluon transverse polarisation vectors proportional to the transverse gluon momenta  $q_{1,2\perp}$  according to Eq. (2.8).

For the evaluation of the scalar master tree- and four-point integrals in the gluon-gluon fusion subprocess we have used the `LoopTools` library [39]. The result is summed up over all possible quark flavors in loops and over distinct loop topologies. We have also checked that the sum of relevant diagrams is explicitly finite and obeys correct asymptotical properties and energy dependence. It is worth to mention that a large cancelation between separate box contributions in the total sum of diagrams takes place, which is expected from the general Standard Model symmetry principles<sup>3</sup>.

---

<sup>3</sup> We are thankful to Prof. O. Nachtmann for an enlightening discussion on this matter.

As soon as the hard subprocess matrix element (denoted above as  $V_{\lambda_+\lambda_-}$ ) has been defined as a function of relevant kinematical variables (four-momenta of incoming/outgoing particles), the loop integration over  $q_{0\perp}$  in Eq. (2.7) was performed to obtain the diffractive amplitude, which then has been used to calculate the differential distributions for (un)polarised  $W$  bosons.

As we will demonstrate below, in the Standard Model the total box contribution is somewhat larger than the triangle one, for the realistic Higgs boson masses. We, however, keep both the triangle and box contributions and investigate a possible interference between them, which, in fact, is quite important, especially at rather large  $W^+W^-$ -pair invariant masses, i.e. in the region we are interested in.

### B. Exclusive $pp \rightarrow pp\gamma\gamma$ process

The same formalism as described above is used to calculate the amplitude for the  $pp \rightarrow pp\gamma\gamma$  process. We write the amplitude of the diffractive  $pp \rightarrow pp\gamma\gamma$  process as

$$\mathcal{M}_{\lambda_+\lambda_-}(s, t_1, t_2) \simeq is \frac{\pi^2}{2} \int d^2\mathbf{q}_{0\perp} V_{\lambda_+\lambda_-}^{gg \rightarrow \gamma\gamma}(q_1, q_2, k_+, k_-) \frac{f_g(q_0, q_1; t_1) f_g(q_0, q_2; t_2)}{\mathbf{q}_{0\perp}^2 \mathbf{q}_{1\perp}^2 \mathbf{q}_{2\perp}^2}, \quad (2.14)$$

where now  $\lambda_{\pm} = \pm 1$  are the helicity polarisation states of the produced photons and corresponding polarisation vectors are defined easily in the  $pp$  center-of-mass frame

$$\epsilon(k, \pm 1) = \frac{1}{\sqrt{2}} (0, i \sin \phi \mp \cos \theta \cos \phi, -i \cos \phi \mp \cos \theta \sin \phi, \pm \sin \theta). \quad (2.15)$$

The typical contributions to the leading order  $gg \rightarrow \gamma\gamma$  subprocess are shown in Fig. 3. The total number of topologically different loop diagrams in the Standard Model amounts to twelve boxes. So the  $\gamma\gamma$  does not exhibit resonant features, and can potentially serve as a probe for New Physics resonant contributions.

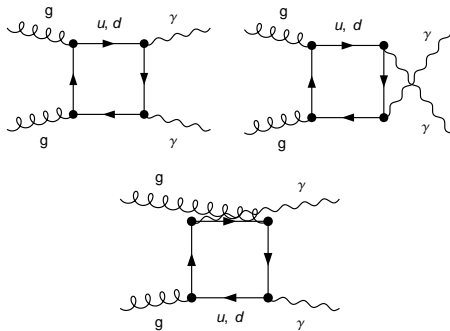


FIG. 3: Representative diagrams of the hard subprocess  $gg \rightarrow \gamma\gamma$ , which contribute to the exclusive  $\gamma\gamma$  pair production.

The box contributions to the  $gg \rightarrow \gamma\gamma$  parton level subprocess amplitude in Fig. 3 for on-shell fusing gluons were calculated analytically by using the Mathematica-based **FormCalc** (FC) [39] package. The complete matrix element was automatically generated by FC tools in terms of one-loop Passarino-Veltman two-, three- and four-point functions and other

internally-defined functions (e.g. gluon and vector bosons polarisation vectors) and kinematical variables.

Other details of the calculation are very much the same as those for the  $W^+W^-$  production. We will not repeat here the details.

### C. Gluon $k_\perp$ -dependent densities in the forward limit

In the  $k_t$ -factorisation approach, the density of gluons in the proton is described in terms of the off-diagonal unintegrated gluon distribution functions (UGDFs)  $f_g(q_0, q_{1,2}; t_{1,2}) = f_g^{\text{off}}(x', x_{1,2}, \mathbf{q}_{0\perp}^2, \mathbf{q}_{1/2\perp}^2, \mu_F^2; t_{1,2})$  at the factorization scale  $\mu_F \sim M_{WW} \gg |\mathbf{q}_{0\perp}|$ . In the forward scattering (see Eq. (2.2)) and asymmetric limit of  $x' \ll x_{1,2}$ , the off-diagonal UGDF is written as a skewedness factor  $R_g(x')$  multiplied by the diagonal UGDF, which describes the coupling of gluons with longitudinal momentum fractions  $x_{1,2}$  to the proton (see Refs. [40, 41] for details). The skewedness parameter  $R_g$  is expected to be roughly constant at LHC energies and gives only a small contribution to the overall normalization uncertainty. We take  $R_g = 1.3$  in practical calculations. In the kinematics considered here, the unintegrated gluon density can be written in terms of the conventional integrated gluon distribution  $g(x, \mathbf{q}_\perp^2)$  as [41]

$$f_g(q_0, q_{1,2}; t_{1,2}) \simeq R_g f_g(x_{1,2}, \mathbf{q}_\perp^2, \mu_F^2) \exp(bt_{1,2}/2) = R_g \frac{\partial}{\partial \ln \mathbf{q}_\perp^2} \left[ x_{1,2} g(x_{1,2}, \mathbf{q}_\perp^2) \sqrt{T_g(\mathbf{q}_\perp^2, \mu_F^2)} \right] \exp(bt_{1,2}/2), \quad (2.16)$$

where the diffractive slope is taken to be  $b = 4 \text{ GeV}^{-2}$ .  $T_g$  is the Sudakov form factor which suppresses real emissions from active gluons during the evolution, so that the rapidity gaps are not populated by gluons. It is given by [41]

$$T_g(\mathbf{q}_\perp^2, \mu_F^2) = \exp\left(-\int_{\mathbf{q}_\perp^2}^{\mu_F^2} \frac{d\mathbf{k}_\perp^2}{\mathbf{k}_\perp^2} \frac{\alpha_s(\mathbf{k}_\perp^2)}{2\pi} \int_0^{1-\Delta} \left[ z P_{gg}(z) + \sum_q P_{qg}(z) \right] dz\right), \quad (2.17)$$

where  $\Delta$  in the upper limit is taken to be [42]

$$\Delta = \frac{|\mathbf{k}_\perp|}{|\mathbf{k}_\perp| + M_{WW}}. \quad (2.18)$$

In our calculations we take  $\mu_F^2 = M_{WW}^2$ . The choice of the scale introduces uncertainties roughly of about factor two. Since in the present calculations we need values of  $T_g(\mathbf{q}_\perp^2, \mu_F^2)$  for extremely large scales  $\mu_F^2$  the integration in Eq. (2.17) is performed rather in  $\log_{10}(k^2/k_0^2)$ , where  $k_0 = 1 \text{ GeV}$  was introduced for convenience.

## III. FOUR-BODY PHASE SPACE IN THE FORWARD LIMIT

The diffractive  $WW$  CEP amplitude (2.7) described above is used now to calculate the corresponding cross section including certain limitations of the phase space. The cross section for the two-boson production can be obtained by integration over the four-body

phase space given by

$$\sigma = \frac{(2\pi)^4}{2s} \int \overline{|\mathcal{M}|^2} \delta^4(p_1 + p_2 - p'_1 - p'_2 - k_+ - k_-) \frac{d^3 p'_1}{(2\pi)^3 2E'_1} \frac{d^3 p'_2}{(2\pi)^3 2E'_2} \frac{d^3 k_+}{(2\pi)^3 2E_+} \frac{d^3 k_-}{(2\pi)^3 2E_-}, \quad (3.1)$$

where  $E'_{1,2}$  and  $E_{\pm}$  are the energies of the final-state protons and produced  $W^{\pm}$  bosons, respectively,  $\overline{|\mathcal{M}|^2} = \sum_{\lambda_+, \lambda_-} \mathcal{M}_{\lambda_+ \lambda_-} \mathcal{M}_{\lambda_+ \lambda_-}^*$  assuming, as usual, that the helicities of both protons are unchanged in the considered process. In order to calculate the total cross section one has to take the eight-dimensional integral numerically (for details see e.g. Ref. [43]). However, the evaluation of the corresponding hard subprocess amplitude  $V_{\lambda_+ \lambda_-}$ , its subsequent convolution with the gluon UPDFs in the diffractive amplitude (2.7) and the full phase space integration (3.1) is extremely time consuming. Clearly the calculation of diffractive mechanism must be simplified to be feasible. Such a simplification seems possible for the diffractive process considered here. We start from the choice of integration variables as in Ref. [43]. Then

$$d\sigma = \frac{1}{2s} \overline{|\mathcal{M}|^2} \frac{1}{2^4} \frac{1}{(2\pi)^8} \frac{1}{E'_1 E'_2} \frac{1}{4} dt_1 dt_2 d\phi_1 d\phi_2 \frac{p_{m\perp}}{4} \mathcal{J}^{-1} dy_+ dy_- dp_{m\perp} d\phi_m, \quad (3.2)$$

where  $p_{m\perp} = |\mathbf{k}_{+\perp} - \mathbf{k}_{-\perp}|$  is the difference between transverse momenta of  $W^+$  and  $W^-$ ,  $\mathbf{k}_{+\perp}$  and  $\mathbf{k}_{-\perp}$ , respectively, and  $\phi_m$  is the corresponding azimuthal angle. For the sake of simplicity, assuming an exponential slope of  $t_1/t_2$ -dependence of the KMR UGDFs (see Eq. (2.16)), and as a consequence of the approximately exponential dependence of the cross section on  $t_1$  and  $t_2$  (proportional to  $\exp(bt_1)$  and  $\exp(bt_2)$ ), the four-body phase space can be calculated as follows

$$d\sigma \approx \left. \frac{1}{2s} \overline{|\mathcal{M}|^2} \right|_{t_{1,2}=0} \frac{1}{2^4} \frac{1}{(2\pi)^8} \frac{1}{E'_1 E'_2} \frac{1}{4} \frac{1}{b^2} (2\pi)^2 \frac{p_{m\perp}}{4} \mathcal{J}^{-1} dy_+ dy_- dp_{m\perp} d\phi_m. \quad (3.3)$$

Since in this approximation we have assumed no correlations between outgoing protons (which is expected here and is practically true for the production of  $b\bar{b}$  [7] or  $g\bar{g}$  [8] dijets) there is no dependence of the integrand in Eq. (3.3) on  $\phi_m$ , which means that the phase space integration can be further reduced to three-dimensional one. The Jacobian  $\mathcal{J}$  in Eq. (3.2) is given in Ref. [43]

$$\mathcal{J} = \left| \frac{p'_{1z}}{\sqrt{m_p^2 + p'^2_{1z}}} - \frac{p'_{2z}}{\sqrt{m_p^2 + p'^2_{2z}}} \right|. \quad (3.4)$$

In actual calculations below we shall use the reduced form of the four-body phase space Eq. (3.3), and it is checked to give correct numerical results against the full phase space calculation for some simple reactions. Different representations of the phase space depending on a particular kinematical distributions needed can be found in Ref. [43].

#### IV. $\gamma\gamma \rightarrow W^+W^-$ MECHANISM

In this section, we briefly discuss the  $\gamma\gamma \rightarrow W^+W^-$  mechanism, considered already in the literature (see Refs. [21, 22]). The relevant subprocess diagrams are shown in Fig. 4.

Let us start from the reminder about the  $\gamma\gamma \rightarrow W^+W^-$  coupling within the Standard Model. The three-boson  $WW\gamma$  and four-boson  $WW\gamma\gamma$  couplings, which contribute to the  $\gamma\gamma \rightarrow W^+W^-$  process in the leading order read

$$\mathcal{L}_{WW\gamma} = -ie(A_\mu W_\nu^- \overset{\leftrightarrow}{\partial}^\mu W^{+\nu} + W_\mu^- W_\nu^+ \overset{\leftrightarrow}{\partial}^\mu A^\nu + W_\mu^+ A_\nu \overset{\leftrightarrow}{\partial}^\mu W^{-\nu}), \quad (4.1)$$

$$\mathcal{L}_{WW\gamma\gamma} = -e^2(W_\mu^- W^{+\mu} A_\nu A^\nu - W_\mu^- A^\mu W_\nu^+ A^\nu), \quad (4.2)$$

where the asymmetric derivative has the form  $X \overset{\leftrightarrow}{\partial}^\mu Y = X \partial^\mu Y - Y \partial^\mu X$ .

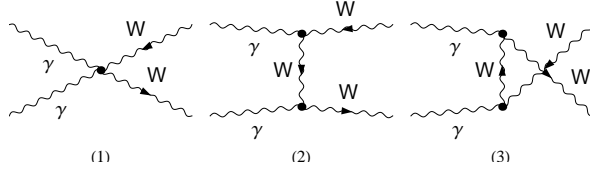


FIG. 4: The Born diagrams for the  $\gamma\gamma \rightarrow W^\pm W^\mp$  subprocess.

Then within the Standard Model, the elementary tree-level cross section for the  $\gamma\gamma \rightarrow W^+W^-$  subprocess can be written in the compact form in terms of the Mandelstam variables (see e.g. Ref. [30])<sup>4</sup>

$$\frac{d\hat{\sigma}}{d\Omega} = \frac{3\alpha^2\beta}{2\hat{s}} \left( 1 - \frac{2\hat{s}(2\hat{s} + 3m_W^2)}{3(m_W^2 - \hat{t})(m_W^2 - \hat{u})} + \frac{2\hat{s}^2(\hat{s}^2 + 3m_W^4)}{3(m_W^2 - \hat{t})^2(m_W^2 - \hat{u})^2} \right), \quad (4.3)$$

where  $\beta = \sqrt{1 - 4m_W^2/\hat{s}}$  is the velocity of the  $W$  bosons in their center-of-mass frame and the electromagnetic fine-structure constant  $\alpha = e^2/(4\pi) \simeq 1/137$  for the on-shell photon. The total elementary cross section can be obtained by integration of the differential cross section above.

In the Weizsäcker-Williams approximation, the total cross section for the  $pp \rightarrow pp(\gamma\gamma) \rightarrow W^+W^-$  can be written as in the parton model

$$\sigma = \int dx_1 dx_2 f_1^{WW}(x_1) f_2^{WW}(x_2) \hat{\sigma}_{\gamma\gamma \rightarrow W^+W^-}(\hat{s}). \quad (4.4)$$

We take the Weizsäcker-Williams equivalent photon fluxes of protons from Ref. [44].

To calculate differential distributions the following parton formula can be conveniently used

$$\frac{d\sigma}{dy_+ dy_- d^2p_{W\perp}} = \frac{1}{16\pi^2 \hat{s}^2} x_1 f_1^{WW}(x_1) x_2 f_2^{WW}(x_2) \overline{|\mathcal{M}_{\gamma\gamma \rightarrow W^+W^-}(\hat{s}, \hat{t}, \hat{u})|^2}, \quad (4.5)$$

<sup>4</sup> This formula does not include the process with virtual Higgs boson  $\gamma\gamma \rightarrow H \rightarrow W^+W^-$  [45]. For heavy Higgs boson, this would lead to clear Higgs boson signal modifying the cross section (typical resonance + background effect) [30], however, with the present limits for Higgs boson mass [33, 34] only deeply off-shell Higgs boson contribution could be possible. Also, the diagram with an intermediate Higgs boson is, of course, of a higher order compared to the contributions considered here. This automatically means rather small effect on the measured cross section, in particular, on the  $W^+W^-$  invariant mass distribution in our case of the four-body  $pp \rightarrow pW^+W^-p$  reaction.

where momentum fractions of the fusing gluons  $x_{1,2}$  are defined in Eq. (2.5). We shall not discuss here any approach beyond the Standard Model. A potentially interesting Higgsless scenario of the  $WW$ -pair production has previously been discussed e.g. in Refs. [21, 22].

In Fig. 5 we show distribution in  $\xi_1 = \log_{10}(x_1)$  and  $\xi_2 = \log_{10}(x_2)$  at  $\sqrt{s} = 14$  TeV. We observe a maximum of the cross section at  $\xi_1, \xi_2 \approx -2$  which means that corresponding longitudinal momentum fractions carried by photons are typically  $10^{-2}$ .

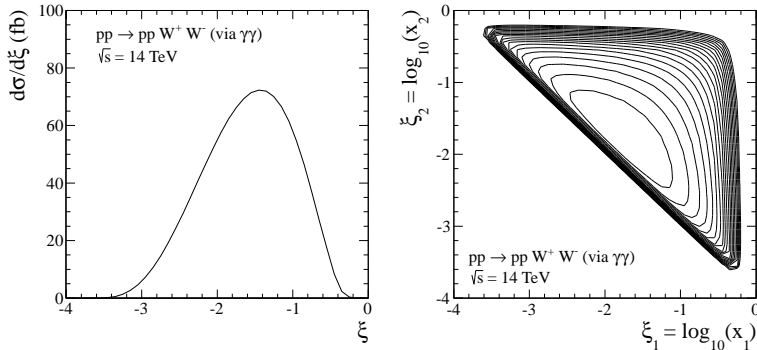


FIG. 5: Summary of the  $\gamma\gamma \rightarrow W^+W^-$  contribution. The lines were calculated within EPA approximation as described in the text with photon fluxes obtained in Ref. [44]. Here,  $\xi_{1,2} = \log_{10}(x_{1,2})$ , where  $x_{1,2}$  are photon longitudinal fractions with respect to parent protons.

## V. INCLUSIVE PRODUCTION OF $W^+W^-$ PAIRS

For a test and for a comparison we also consider a gluon-gluon contribution to the inclusive cross section. We are not interested in the quark-antiquark component which is simple and well known. We also omit  $pp \rightarrow t\bar{t}X \rightarrow W^+W^-b\bar{b}X$  process very important at high energy. In the lowest order of pQCD the inclusive cross section for the gluon-gluon fusion can be written as

$$\frac{d\sigma^{gg}}{dy_+ dy_- d^2p_{W\perp}} = \frac{1}{16\pi^2 \hat{s}^2} x_1 g(x_1, \mu_F^2) x_2 g(x_2, \mu_F^2) \overline{|\mathcal{M}_{gg \rightarrow W^+W^-}(\lambda_1, \lambda_2, \lambda_+, \lambda_-)|^2}. \quad (5.1)$$

The corresponding matrix elements have been discussed in the literature in detail [27]. The distributions in rapidity of  $W^+$  ( $y_+$ ), rapidity of  $W^-$  ( $y_-$ ) and transverse momentum of one of them  $p_{W\perp}$  can be calculated in a straightforward way from Eq. (5.1). The distribution in invariant mass can be then obtained by an appropriate binning. Our inclusive  $d\sigma/dM_{WW}$  distribution seems consistent with similar distributions presented in the past in the literature.

The total cross section can be obtained from a simpler formula:

$$\sigma_{pp \rightarrow W^+W^-X}^{gg} = \int dx_1 dx_2 g(x_1, \mu_F^2) g(x_2, \mu_F^2) \hat{\sigma}_{gg \rightarrow W^+W^-}(\hat{s}). \quad (5.2)$$

Let us concentrate for a while a the elementary  $gg \rightarrow W^+W^-$  cross section shown in Fig.6. In this calculation we have assumed  $m_{h^0} = 125$  GeV [28]. We also show a vertical line at the  $t\bar{t}$  threshold. The figure demonstrates a cancellation pattern between box and triangle contributions. We will discuss similar cancellation for the  $pp \rightarrow ppW^+W^-$  reaction in the

next section. We wish to notice that  $\hat{\sigma}_{gg \rightarrow W^+W^-} \ll \hat{\sigma}_{\gamma\gamma \rightarrow W^+W^-} \xrightarrow{\hat{s} \rightarrow \infty} \sim 10^2$  pb. This shows a potential role of photon-photon induced processes of  $W^+W^-$  production not discussed so far in the context of inclusive process.

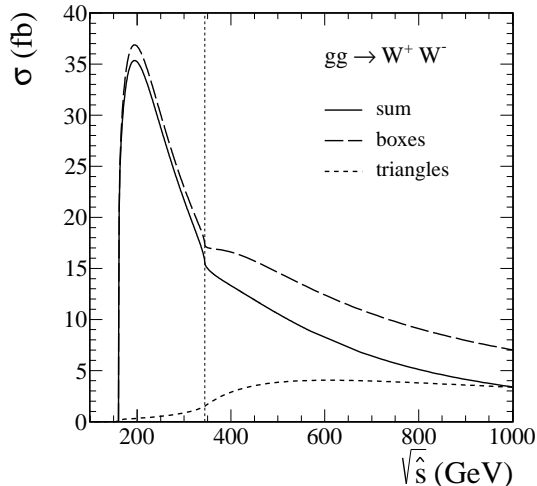


FIG. 6: The integrated elementary cross section for the  $gg \rightarrow W^+W^-$  reaction. The solid line represents the coherent sum of all contributions. We show separate contributions of boxes (dashed line) and triangles (dotted line).

As discussed before, in the case of exclusive scattering the  $J_z = 0$  contribution is the dominant one. In the case of inclusive process the situation is slightly different. In Fig.7 we present the  $J_z = 0$  and  $|J_z| = 2$  components to angular distributions. The  $J_z = 0$  contribution is generally larger than the  $|J_z| = 2$  one. As in the exclusive case, at forward scattering ( $\cos \theta = \pm 1$ ) we observe the dominance of the  $J_z = 0$  contribution. At  $\sqrt{\hat{s}} = 500$  GeV it happens very close to  $\cos \theta \approx \pm 1$ .

For completeness in Fig.8 we show corresponding contributions to the rapidity distribution of one of  $W$ 's in the  $pp \rightarrow W^+W^-X$  process. Here the  $J_z = 0$  contribution is larger in the whole range of rapidities.

## VI. RESULTS

Before we go to the presentation of results for the  $pp \rightarrow ppW^+W^-$  reaction we wish to show results for the  $p\bar{p} \rightarrow p\bar{p}\gamma\gamma$  reaction. The latter reaction was studied experimentally in Ref.[20].

### A. $pp \rightarrow pp\gamma\gamma$

The  $p\bar{p} \rightarrow p\bar{p}\gamma\gamma$  process was discussed recently in [46]. No differential distributions have been discussed there. The CDF Collaboration has measured photons in the interval  $|\eta(\gamma)| < 1.0$ ,  $E_T > 2.5$  GeV and with the condition of no other particles detected in  $-7.4 < \eta < 7.4$ . They have obtained  $\sigma_{\gamma\gamma} = 2.48$  pb with about quarter of relative uncertainty. We obtain 2.99 pb for the GJR NLO gluon distribution [47], 2.46 pb for the MSTW08 NLO gluon

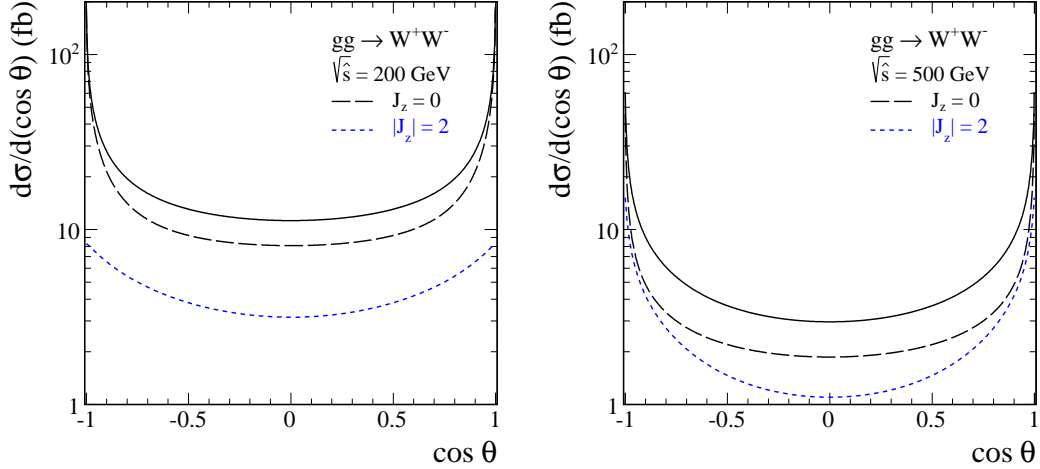


FIG. 7: Centre-of-mass scattering angle dependence of the hard subprocess  $gg \rightarrow W^+W^-$  cross section averaged over incoming gluon polarizations. The solid line represents the coherent sum of all contributions. The  $J_z = 0$  (dashed line) and the  $|J_z| = 2$  (dotted line) contributions are shown separately.

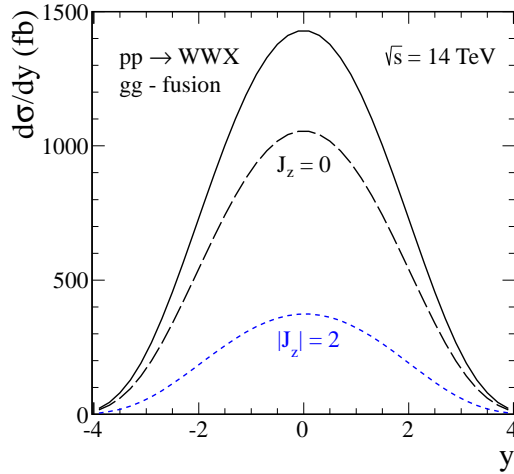


FIG. 8: The  $J_z = 0$  (dashed line) and  $|J_z| = 2$  (dotted line) contributions to the inclusive  $pp \rightarrow W^+W^-X$  rapidity distribution.

distribution [48] and 2.1 pb for the CT12 NLO gluon distribution [49]. Our results very well agree with the CDF experimental data. In this calculation we have assumed averaged soft gap survival factor  $S_g = 0.05$  and the scale of the Sudakov form factor was taken as  $\mu^2 = M_{\gamma\gamma}^2$ . Cuts on the gluon transverse momenta  $q_{\perp, cut}^2 = 0.5 \text{ GeV}^2$  were imposed.

In Fig.9 (left panel) we show distribution of photon-photon invariant mass with experimental CDF cuts. We show results for three different gluon distributions [47–49]. We obtain very good description of the CDF experimental data [20], both in shape and absolute normalization. In the right panel we show corresponding distribution in photon transverse momentum.

Finally in Fig.10 we show corresponding distribution in photon pseudorapidity in the left

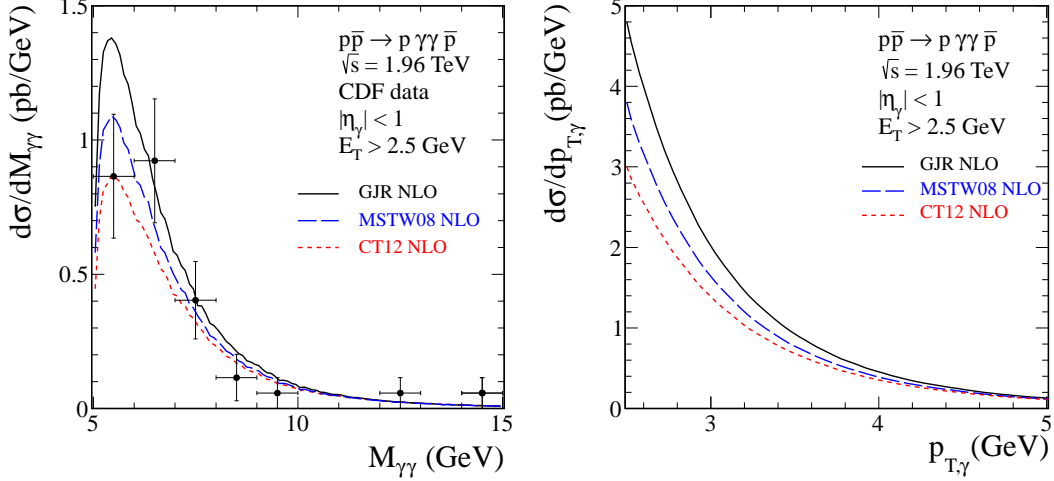


FIG. 9: Left panel: Photon-photon invariant mass distribution. We show results for three different gluon distributions specified in the figure. The experimental data are taken from Ref.[20]. Right panel:

panel, again for three different gluon distributions. In the right panel we present decomposition into different  $pp$  center-of-mass photon helicity components.

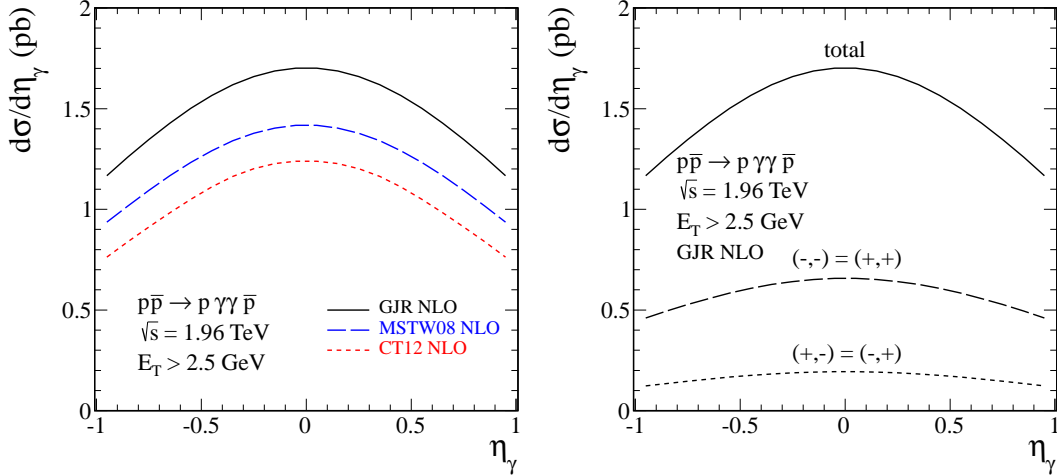


FIG. 10: Distribution in photon pseudorapidity for three different gluon distributions (left panel) and the decomposition into different  $pp$  center-of-mass photon helicity components.

Having shown that the results of the approach used in the present paper nicely describe the CDF experimental data [20] we can confidentially present our predictions for the  $pp \rightarrow ppW^+W^-$  reaction.

### B. $pp \rightarrow ppW^+W^-$

Let us present now our results for the central exclusive  $W^+W^-$  pair production. In Fig. 11 we compare rapidity distribution of  $W^+$  (or  $W^-$ ) for the electromagnetic  $\gamma\gamma \rightarrow W^+W^-$

and diffractive  $gg \rightarrow W^+W^-$  mechanisms. The two-photon induced contribution is almost three orders of magnitude larger than the diffractive contribution, in which all polarization components for  $W^+$  and  $W^-$  have been included. For a reference, we show also inclusive cross section ( $gg \rightarrow W^+W^-$  contribution only) which is roughly two more orders of magnitude bigger than the exclusive  $\gamma\gamma \rightarrow W^+W^-$  contribution. We see, therefore, that the exclusive diffractive component is five orders of magnitude smaller for its inclusive counterpart. The diffractive contribution was calculated with the GJR NLO [47] collinear gluon distribution, in order to generate the off-diagonal UGDFs given by Eq. (2.16). This collinear PDF allows us to use quite small values of gluon transverse momenta ( $q_{\perp, cut}^2 = 0.5 \text{ GeV}^2$ ).

A much smaller diffractive contribution compared to the two-photon one requires a special comment as it is rather exceptional. For example, it is completely opposite than for  $pp \rightarrow ppH$  [7],  $pp \rightarrow ppM$  (e.g. light/heavy quarkonia production [9, 10]) or  $pp \rightarrow ppQ\bar{Q}$  [7, 50] CEP processes. The standard relative suppression, present also in the latter cases, is due to soft gap survival probability factor ( $S_g \sim 0.03$  for diffractive contribution versus  $S_g \sim 1$  for two-photon contribution), and due to a suppression by the Sudakov form factor calculated at very large scales, here at  $\mu_{hard} = M_{WW}$ . The main difference compared to other cases is that in the diffractive case the leading contribution comes from loop diagrams while in the two-photon case already from tree level diagrams.

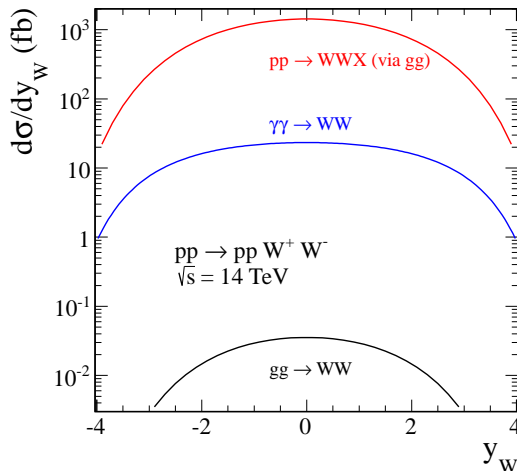


FIG. 11: Rapidity distribution of  $W$  bosons. The diffractive contribution is shown by the bottom line while the  $\gamma\gamma \rightarrow W^+W^-$  contribution by the middle line. For comparison, we also show the cross section for the inclusive ( $gg$ -fusion only) production case (upper line).

In Fig. 12 we present, in addition, individual polarization components for the diffractive mechanism, along with the unpolarized cross section. The calculation of the helicity contributions is performed in the  $pp$  center-of-mass frame (in which all the experimental studies of the exclusive production processes are usually performed). As can be seen from the figure, the contribution of  $(\lambda_+, \lambda_-) = (\pm 1, \mp 1)$  is bigger than other contributions and the contribution of  $(\lambda_+, \lambda_-) = (\pm 1, \pm 1)$  concentrated mostly at midrapidities. Since we use  $pp$  center of mass helicities there is on simple relation to the often used in a qualitative discussion  $J_z = 0$  dominance rule. Discussion of the  $J_z = 0$  rule would require complicated transformations between different reference frames and going beyond approximations made here. This clearly goes beyond the scope of this paper. In particular, as it is seen from

Fig. 12 the helicity contributions obey the following relation

$$\frac{d\sigma_{\lambda\lambda'}(y_+)}{dy_+} = \frac{d\sigma_{\lambda'\lambda}(y_-)}{dy_-}, \quad (6.1)$$

where  $y_{\pm}$  are rapidities of  $W^{\pm}$  bosons, respectively. The unpolarized cross section does not show up any peculiarities in  $y$ -dependence and is symmetric with respect to  $y = 0$  for both  $W^+$  and  $W^-$  bosons.

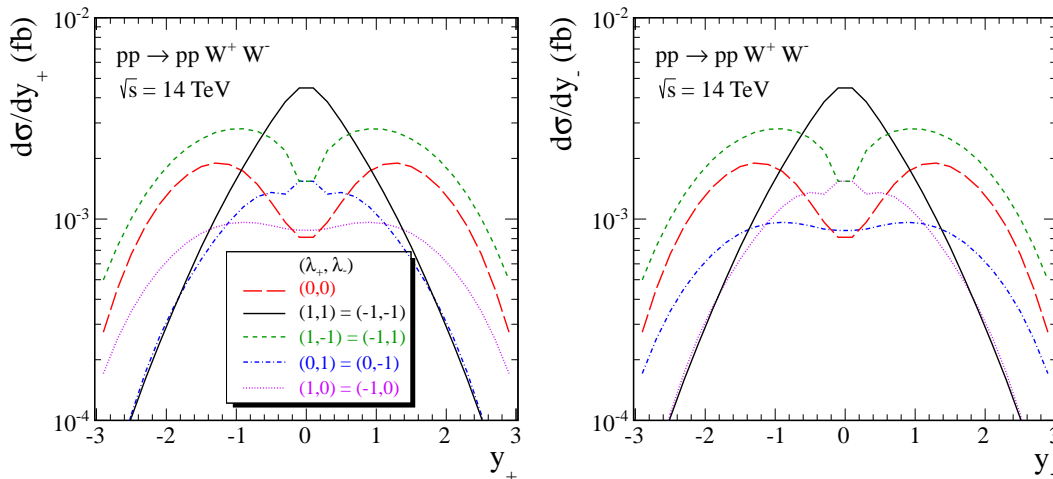


FIG. 12: Rapidity distribution of separate polarisation components to the diffractive  $W$  bosons production. The individual contributions are marked in the figure.

In Fig. 13 we show distribution in  $W^+$  ( $W^-$ ) transverse momentum. The distribution for exclusive diffractive production is much steeper than that for the electromagnetic contribution. A side remark is in order here. The diffractive contribution peaks at  $p_{t,W} \sim 25$  GeV. This is somewhat smaller than for the  $\gamma\gamma \rightarrow W^+W^-$  mechanism where the maximum is at  $p_{t,W} \sim 40$  GeV. The exclusive cross section for photon-photon contribution is at large transverse momenta  $\sim 1$  TeV smaller only by one order of magnitude than the inclusive  $gg \rightarrow W^+W^-$  component. The situation could be even more favorable if New Physics would be at the game [21].

Fig. 14 shows distribution in the  $W^+W^-$  invariant mass which is particularly important for the New Physics searches at the LHC [21]. The distribution for the diffractive component drops quickly with the  $M_{WW}$  invariant mass. For reference and illustration, we show also distribution when the Sudakov form factors in Eq. (2.16) is set to one. As can be seen from the figure, the Sudakov form factor lowers the cross section by a large factor. The damping is  $M_{WW}$ -dependent as can be seen by comparison of the two curves. The larger  $M_{WW}$  the larger the damping. We show the full result (boxes + triangles) and the result with boxes only which would be complete if the Higgs boson does not exist. At high invariant masses, the interference of boxes and triangles decreases the cross section. The distribution for the photon-photon component drops very slowly with  $M_{WW}$  and at  $M_{WW} > 1$  TeV the corresponding cross section is even bigger than the  $gg \rightarrow W^+W^-$  component to inclusive production of  $W^+W^-$  pairs.

Finally, in Fig. 15 we show for completeness the two-dimensional distributions in rapidities of  $W^+/W^-$  bosons in both electromagnetic and QCD mechanisms. We see a typical

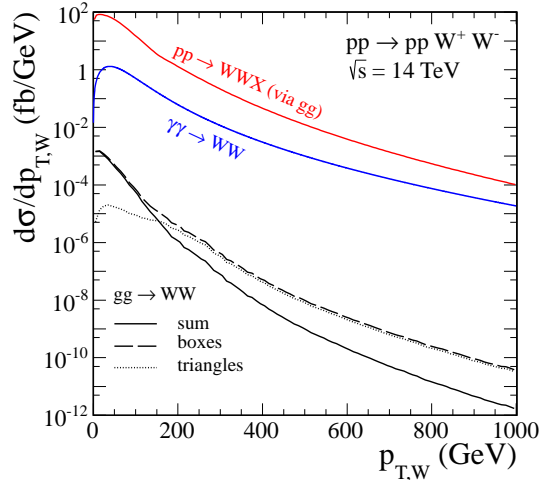


FIG. 13: Distribution in transverse momentum of one of the  $W$  bosons. The diffractive contribution is shown by the bottom solid line while the  $\gamma\gamma \rightarrow W^+W^-$  contribution by the middle solid line. The top solid line corresponds to the inclusive two-gluon initiated  $pp \rightarrow W^+W^-X$  component. Separate contributions of boxes (dashed) and triangles (dotted) are shown in addition for illustrating the cancellation effect.

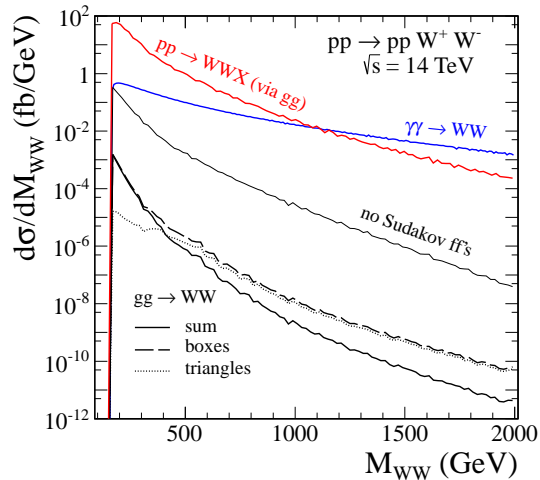


FIG. 14: Distribution in  $W^+W^-$  invariant mass. We show both the QCD diffractive contribution and the electromagnetic  $\gamma\gamma \rightarrow W^+W^-$  contribution. The result when the Sudakov form factor is put to one is shown for illustration of its role. The most upper curve is for the inclusive gluon-initiated  $pp \rightarrow W^+W^-X$  component.

correlation pattern characteristic for  $2 \rightarrow 2$  subprocesses. This distribution does not show any specific behavior which could be used to differentiate the diffractive and the two-photon contributions.

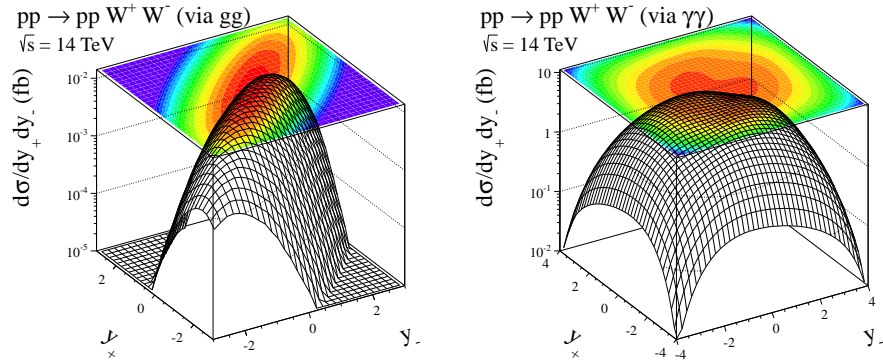


FIG. 15: Two-dimensional distribution in rapidity of  $W^+$  and  $W^-$  bosons for the diffractive mechanism (left panel) and two-photon mechanism (right panel).

## VII. CONCLUSIONS

We have calculated the QCD diffractive contribution to the exclusive  $pp \rightarrow pW^+W^-p$  process for the first time in the literature with the full one-loop  $gg \rightarrow W^+W^-$  matrix element. Two mechanisms have been considered. First mechanism is a virtual (highly off-shell) Higgs boson production and its subsequent transformation into real  $W^+W^-$  pair. Second mechanism relies on the formation of intermediate quark boxes, very much similar to ones in the exclusive two photon production mechanism.

We have calculated corresponding amplitudes using computer program package `FormCalc`. We have made a first estimate of the cross section using amplitudes in the forward limit “corrected” off-forward via a simple exponential (slope dependent) extrapolation.

In order to gain confidence to our calculations and the formalism used we consider also the  $p\bar{p} \rightarrow p\bar{p}\gamma\gamma$  process which was measured recently by the CDF Collaboration. Here the formalism of calculating quark box diagrams is essentially the same as for the exclusive production of  $W^+W^-$  pairs. We have obtained very nice agreement with experimental diphoton invariant mass distribution.

Having verified the formalism for diphoton production we have performed similar calculation for  $W^+W^-$  production. Differential distributions in the  $W^\pm$  transverse momentum, rapidity and  $W^+W^-$  pair invariant mass have been calculated and compared with corresponding distributions for discussed in the literature  $\gamma\gamma \rightarrow W^+W^-$  mechanism. The contribution of triangles with the intermediate Higgs boson turned out to be smaller than the contribution of boxes taking into account recent very stringent limitations on Higgs boson mass from Tevatron and LHC data. We have found that, in contrast to exclusive production of Higgs boson or dijets, the two-photon fusion dominates over the diffractive mechanism for small four-momentum transfers squared in the proton lines ( $t_1, t_2$ ) as well as in a broad range of  $W^+W^-$ -pair invariant masses, in particular, for large  $M_{WW}$ . Estimated theoretical uncertainties cannot disfavor this statement. The large  $M_{WW}$  region is damped in the diffractive model via scale dependence of the Sudakov form factor.

One could focus on the diffractive contribution by imposing lower cuts on  $t_1$  and/or  $t_2$  using very forward detectors on both sides of the interaction point at distances of 220 m and

420 m as planned for future studies at ATLAS and CMS. The corresponding cross section is, however, expected to be extremely low.

Compared to the previous studies in the effective field theory approach, in this work we have included the complete one-loop (leading order)  $gg \rightarrow W^+W^-$  matrix element, and have shown that extra box diagrams, even though they are larger than the resonant (s-channel Higgs) diagrams, constitute a negligibly small background for a precision study of anomalous couplings.

The unique situation of the dominance of the  $\gamma\gamma \rightarrow W^+W^-$  contribution over the diffractive one opens a possibility of independent tests of the Standard Model as far as the triple-boson  $\gamma WW$  and quartic-boson  $\gamma\gamma WW$  coupling is considered. It allows also for stringent tests of some Higgsless models as discussed already in the literature (see e.g. Ref. [21]).

### VIII. ACKNOWLEDGMENTS

Useful discussions with Rikard Enberg, Gunnar Ingelman, Valery Khoze, Otto Nachtmann, Christophe Royon, Torbjörn Sjöstrand and Marek Tasevsky are gratefully acknowledged. This study was partially supported by the MNiSW grants No. DEC-2011/01/N/ST2/04116 and DEC-2011/01/B/ST2/04535. Authors are grateful to the European Center for Theoretical Studies in Nuclear Physics and Related Areas (ECT\*, Trento, Italy) for warm hospitality during their stay when this work was completed. Piotr Lebiedowicz is thankful to the THEP Group at Lund University (LU), Sweden, for hospitality during his collaboration visit at LU.

- 
- [1] A. Schäfer, O. Nachtmann and R. Schöpf, Phys. Lett. **B249** (1990) 331.
  - [2] A. Bialas and P. V. Landshoff, Phys. Lett. **B256** (1991) 540.
  - [3] M. G. Albrow, T. D. Coughlin and J. R. Forshaw, Prog. Part. Nucl. Phys. **65** (2010) 149.
  - [4] M. G. Albrow *et al.* (FP420 R&D Collaboration), JINST **4**, T10001 (2009).
  - [5] M. G. Albrow and A. Rostovtsev, arXiv:0009336 [hep-ph].
  - [6] V. A. Khoze, A. D. Martin and M. G. Ryskin, Phys. Lett. **B401** (1997) 330;  
V. A. Khoze, A. D. Martin and M. G. Ryskin, Eur. Phys. J. **C14** (2000) 525;  
V. A. Khoze, A. D. Martin and M. G. Ryskin, Eur. Phys. J. **C19** (2001) 477 [Erratum-ibid. **C20** (2001) 599];  
V. A. Khoze, A. D. Martin and M. G. Ryskin, Eur. Phys. J. **C23** (2002) 311;  
A. B. Kaidalov, V. A. Khoze, A. D. Martin and M. G. Ryskin, Eur. Phys. J. **C33** (2004) 261.
  - [7] R. Maciula, R. Pasechnik and A. Szczurek, Phys. Rev. **D82** (2010) 114011;  
R. Maciula, R. Pasechnik and A. Szczurek, Phys. Rev. **D83** (2011) 114034.
  - [8] R. Maciula, R. Pasechnik and A. Szczurek, Phys. Rev. **D84** (2011) 114014.
  - [9] R. S. Pasechnik, A. Szczurek and O. V. Teryaev, Phys. Rev. **D78** (2008) 014007;  
R. S. Pasechnik, A. Szczurek and O. V. Teryaev, Phys. Lett. **B680** (2009) 62;  
R. S. Pasechnik, A. Szczurek and O. V. Teryaev, Phys. Rev. **D81** (2010) 034024;  
R. Pasechnik, A. Szczurek and O. Teryaev, Phys. Rev. **D83** (2011) 074017;  
P. Lebiedowicz, R. Pasechnik and A. Szczurek, Phys. Lett. **B701** (2011) 434.
  - [10] L. A. Harland-Lang, V. A. Khoze, M. G. Ryskin and W. J. Stirling, Eur. Phys. J. **C69** (2010) 179.

- [11] J. R. Cudell, A. Dechambre, O. F. Hernandez and I. P. Ivanov, *Eur. Phys. J.* **C61** (2009) 369.
- [12] A. Dechambre, O. Kepka, C. Royon and R. Staszewski, *Phys. Rev.* **D83** (2011) 054013.
- [13] V. A. Khoze, M. G. Ryskin and W. J. Stirling, *Eur. Phys. J.* **C48** (2006) 477.
- [14] R. Pasechnik, R. Enberg and G. Ingelman, *Phys. Rev.* **D82** (2010) 054036;  
R. Pasechnik, R. Enberg and G. Ingelman, *Phys. Lett.* **B695** (2011) 189.
- [15] M. G. Ryskin, A. D. Martin, V. A. Khoze, *Eur. Phys. J.* **C60** (2009) 265.
- [16] A. Szczurek, R. S. Pasechnik and O. V. Teryaev, *Phys. Rev.* **D75** (2007) 054021.
- [17] L. A. Harland-Lang, V. A. Khoze, M. G. Ryskin and W. J. Stirling, *Eur. Phys. J.* **C71** (2011) 1714.
- [18] R. Enberg and R. Pasechnik, *Phys. Rev.* **D83** (2011) 095020.
- [19] T. Aaltonen *et al.* (CDF Collaboration), *Phys. Rev. Lett.* **99** (2007) 242002;  
T. Aaltonen *et al.* (CDF Collaboration), *Phys. Rev.* **D77** (2008) 052004;  
T. Aaltonen *et al.* (CDF Collaboration), *Phys. Rev. Lett.* **102** (2009) 242001.
- [20] T. Aaltonen *et al.* (CDF Collaboration), *Phys. Rev. Lett.* **108** (2012) 081801.
- [21] O. Kepka and C. Royon, *Phys. Rev.* **D78** (2008) 073005;  
E. Chapon, C. Royon and O. Kepka, *Phys. Rev.* **D81** (2010) 074003.
- [22] N. Schul and K. Piotrkowski, *Nucl. Phys. B (Proc. Suppl.)* **179-180** (2008) 289;  
T. Pierzchała and K. Piotrkowski, *Nucl. Phys. B (Proc. Suppl.)* **179-180** (2008) 257.
- [23] M. Maniatis, A. v. Manteuffel and O. Nachtmann, *Nucl. Phys. B (Proc. Suppl.)* **179-180** (2008) 104.
- [24] O. Nachtmann, F. Nagel, M. Pospischil and A. Utermann, *Eur. Phys. J.* **C45** (2005) 679; *Eur. Phys. J.* **C46** (2006) 93.
- [25] B. E. Cox, A. De Roeck, V. A. Khoze *et al.*, *Eur. Phys. J.* **C45** (2006) 401.
- [26] R. S. Gupta, *Phys. Rev.* **D85** (2012) 014006.
- [27] E. W. N. Glover and J. J. van der Bij, *Phys. Lett.* **B219** (1989) 488;  
Ch. Kao and D. A. Dicus, *Phys. Rev.* **D43** (1991) 1555.
- [28] G. Aad *et al.* (ATLAS Collaboration), *Phys. Lett.* **B716** (2012) 1;  
S. Chatrchyan *et al.* (CMS Collaboration), *Phys. Lett.* **B716** (2012) 30.
- [29] S. Y. Choi and F. Schrempp, *Phys. Lett.* **B272** (1991) 149;  
E. Yehudai, *Phys. Rev.* **D44** (1991) 3434;  
G. Belanger and F. Boudjema, *Phys. Lett.* **B288** (1992) 210.
- [30] A. Denner, S. Dittmaier and R. Schuster, *Nucl. Phys.* **B452** (1995) 80.
- [31] K. Nakamura *et al.* (Particle Data Group), *J. Phys.* **G37** (2010) 075021.
- [32] The TEVNP Working Group for the CDF and D0 Collaborations, FERMILAB-CONF-11-372-E, arXiv:1108.3331 [hep-ex].
- [33] ATLAS Collaboration, ATLAS-CONF-2011-163; CERN-PH-EP-2011-190, *Phys. Rev. Lett.* **108** (2012) 111802.
- [34] CMS Collaboration, CMS PAS HIG-11-032; CMS-HIG-11-024, *Phys. Lett.* **B710** (2012) 91.
- [35] V. I. Kuksa and R. S. Pasechnik, *Int. J. Mod. Phys.* **A24** (2009) 5765;  
R. S. Pasechnik and V. I. Kuksa, *Mod. Phys. Lett.* **A26** (2011) 1075.
- [36] G. Passarino, *Nucl. Phys.* **B488** (1997) 3.
- [37] R. S. Pasechnik, O. V. Teryaev and A. Szczurek, *Eur. Phys. J.* **C47** (2006) 429.
- [38] R. Enberg, R. Pasechnik and O. Stål, *Phys. Rev.* **D85** (2012) 075016.
- [39] T. Hahn, *Comput. Phys. Commun.* **140** (2001) 418;  
T. Hahn and M. Perez-Victoria, *Comput. Phys. Commun.* **118** (1999) 153;  
T. Hahn, *Comput. Phys. Commun.* **178** (2008) 217.

- [40] M. A. Kimber, A. D. Martin and M. G. Ryskin, Phys. Rev. **D63** (2001) 114027.
- [41] A. D. Martin and M. G. Ryskin, Phys. Rev. **D64** (2001) 094017.
- [42] T. D. Coughlin and J. R. Forshaw, JHEP **1001** (2010) 121.
- [43] P. Lebiedowicz and A. Szczurek, Phys. Rev. **D81** (2010) 036003.
- [44] M. Drees and D. Zeppenfeld, Phys. Rev. **D39** (1989) 2536.
- [45] M. A. Shifman, A. I. Vainshtein, M. B. Voloshin and V. I. Zakharov, Sov. J. Nucl. Phys. **30** (1979) 711;  
 E. E. Boos and G. V. Jikia, Phys. Lett. **B275** (1992) 164;  
 D. A. Morris, T. N. Troung and D. Zappala, Phys. Lett. **B323** (1994) 421;  
 H. Veltman, Z. Phys. **C62** (1994) 235.
- [46] L.A. Harland-Lang, V.A. Khoze, M.G. Ryskin and W.J. Stirling, arXiv:1204.4803 [hep-ph].
- [47] M. Glück, D. Jimenez-Delgado and E. Reya, Eur. Phys. J. **C53** (2008) 355;  
 M. Glück, D. Jimenez-Delgado, E. Reya and C. Schuck, Phys. Lett. **B664** (2008) 133.
- [48] A.D. Martin, W.J. Stirling, R.S. Thorne and G. Watt, Eur. Phys. J. **C63** (2009) 189;  
 G. Watt and R.S. Thorne, arXiv: 1205.4024 [hep-ph].
- [49] H.-L. Lai *et al.*, Phys. Rev. **D82** (2010) 074024.
- [50] R. Maciula, R. Pasechnik and A. Szczurek, Phys. Lett. **B685** (2010) 165.